

# Effect of Axial Guard Electrodes on Sensing Field of Capacitance Tomographic Sensor

Hui Xu<sup>#</sup>, Gang Yang and Shi Wang

PO Box 321, School of Information Science and Engineering,  
Northeastern University, Shenyang, 110006, P. R. China

<sup>#</sup> E-mail: cxscxsc@pub.sy.ln.cn

Tel: +86 24 25416000

**Abstract** –Electrical capacitance tomography is now used in many industrial processes for visualizations. There are several types of sensor structures in using in the tomographic systems. The knowledge of their three-dimensional effects of these structures is important. In this paper the results of relevant analyses are given by use of the numerical method Finite Element Method (FEM). At last images with different sensor structures are reconstructed and the corresponding Spatial Image Errors (SIE) are given.

**Keywords:** electrical capacitance tomography, guard electrode, sensing field, three-dimension

## 1. INTRODUCTION

Electrical Capacitance Tomography (ECT) systems are the first tomographic system being developed and commercially used in industrial processes for multi-phase-flow measurements. In some occasions there is the need of visualizing the density distributions of materials inside a black object, such as a fluidized bed, a chemical reactor, a fractional column and so on, therefore sensors with multi-level structures are designed [1-4]. When the two-dimensional images of cross-sections from each level are reconstructed, the three-dimensional images inside the black object are obtained by piling up these 2D images. The analyses of the capacitance electrode array are important for mastering the properties of the sensors. Finite element method (FEM) is proved to be an effective manner to simulate the sensor structures. For these multi-level sensor structures, three-dimensional analyses must be proceeded to obtain the sensors' properties in detail.

In this paper three types of sensor structures which can be used in visualizing the three-dimensional situation of a black object are analyzed. The authors first analyzed the axial sensitivity attenuation and the capacitance changes of different sensor structures at certain positions. From that the axial sensing fields are drawn. Then the cross-sectional sensitivity distributions at the measurement electrode level are shown. In the end, images with these structures are reconstructed toward a certain physical phantom, and the corresponding Spatial Image Error (SIE) are calculated.

## 2. SENSOR STRUCTURES

When ECT systems are used to visualizing a black object, several sensor structures can be chosen from. One is a multi-level electrode sensor array with same electrode size evenly mounted on the surface of the inner or outer wall of the container.

In the multi-level electrode sensor types, as one electrode level is acted as measurement electrodes, the other electrodes other than the measurement electrodes are acted as axial guards. The guard electrodes usually have two selectable potentials: zero potential or potential applied the same as the active electrode. When the corresponding electrodes being at the same position as the active electrode of the measurement level in the cross sections are made the same potential with the active electrode, this kind of sensor structure is called driven axial guards. This is called sensor type 1. When the guard electrodes are all at zero potentials, this kind of sensor structure is called earthed axial guard rings. This is called sensor type 2 in this paper.

The another sensor structure is a one-level electrode sensor array without any axial guard which can measure different position's 2D cross-sectional distributions by moving the sensor array along the axial direction. This is called sensor type 3 in this paper.

The above three types of sensor structures are schematically shown in Figure 1 in which there are 8 electrodes in each measurement level mounted on the inner wall of the container. And the whole sensor unit is wrapped by an earthed screen to prevent external noise. Where  $h$  is the height of the electrodes,  $d$  is the distance

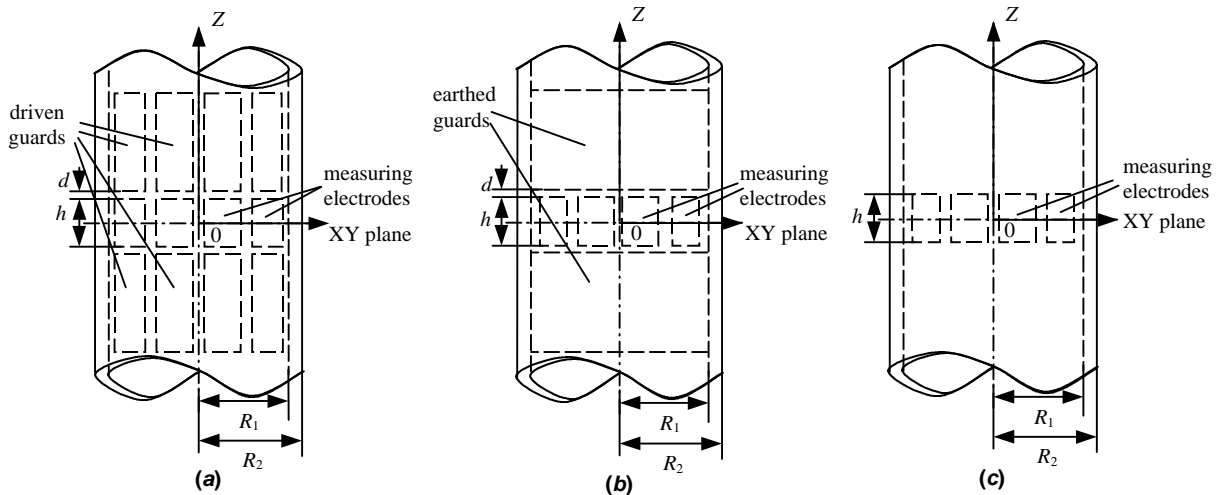


Figure 1: Schematic diagram of three types of sensor structures

- (a) Sensor with driven axial guards;
- (b) Sensor with earthed axial guard rings;
- (c) Sensor without any axial guard

between the two electrode levels.  $Z$  is axial direction.  $R_1$  and  $R_2$  are the inner and the outer radius of the container respectively. And  $R_3$  the radius of the earthed screen.

### 3. AXIAL SENSITIVITY DISTRIBUTION

The sensitivity attenuation curves along axial direction at two positions, i.e. near the active electrode and near the  $Z$ -axis, are drawn in Figure 2. The  $S_{15}(e)$  denotes the sensitivity of the capacitance of electrodes 1 and 5 to the changes of high permittivity material near the active electrode. And the  $S_{15}(m)$  is that of electrodes 1 and 5 to the material presented near the  $Z$ -axis. In the simulations, the relative structure parameters are:  $R_1 = 0.125m$ , the permittivity of the container wall  $\epsilon_w = 8$ , and the subtended angle of the electrodes  $\theta = 10^\circ$ . In all these figures, curve 1 is under the condition of  $R_2 = 1.1R_1$ ,  $R_3 = 1.25R_1$ , curve 2 is  $R_2 = 1.15R_1$ ,  $R_3 = 1.2R_1$ , and curve 3 is  $R_2 = 1.05R_1$ ,  $R_3 = 1.15R_1$ .

By the analyses the sensitivity attenuation along the axial direction of type 1 is the slowest among these three types. This means the sensing field of this kind of sensor structure is much wider than the measurement electrode area. On the contrast, the sensing field of type 2, i.e. the sensor structure with earthed axial guard rings, is narrowed to a smaller range. But it should be noted that there are negative sensing fields beside it in the axial direction when the measurement electrode level is closer to the earthed guard electrode levels. And the sensing

field of type 3 is nearly the same as that of type 2. Figure 3 shows the sensing fields of type 1 and type 2 on axial section.

### 4. CAPACITANCE CHANGES

When the absolute capacitance changes related to the capacitance measurement circuit are observed, it can be found that  $(C(k) - C_0)$  of sensor type 2 is several times smaller than that of the other two types. Among them, the  $(C(k) - C_0)$  of sensor type 3 is the biggest when  $k$  is not at the position near the detecting electrode (this will be stated in the following section). This should be taken into account when the resolution of the capacitance measurement circuit is limited.

### 5. CROSS SECTIONAL SENSITIVITY DISTRIBUTIONS

The cross sectional sensitivity distributions of these three types are calculated by use of 3D FEM, only two groups of them are given in Figure 4. And the distributions of type 3 are the same as them of type 2. From the results of simulations, the distributions of type 1 are special. In this driven guard structure, the sensitivities at symmetrical positions of the active electrode and detecting electrode are not equal. The values near the detecting electrode are nearly 10 times larger than that near the active electrode. Therefore, the sensitivity attenuation along the axial direction near the detecting electrode is different from that of active electrode. The

attenuation curve is like that of type 2, also with negative sensing fields beside it in the axial direction when the measurement electrode level is closer to the guard electrode levels. The results imply that although the electric flux lines

of the electrostatic field are straight and the stresses are equal everywhere on the axial-radial section through the Z-axis, sensitivities are not the same.

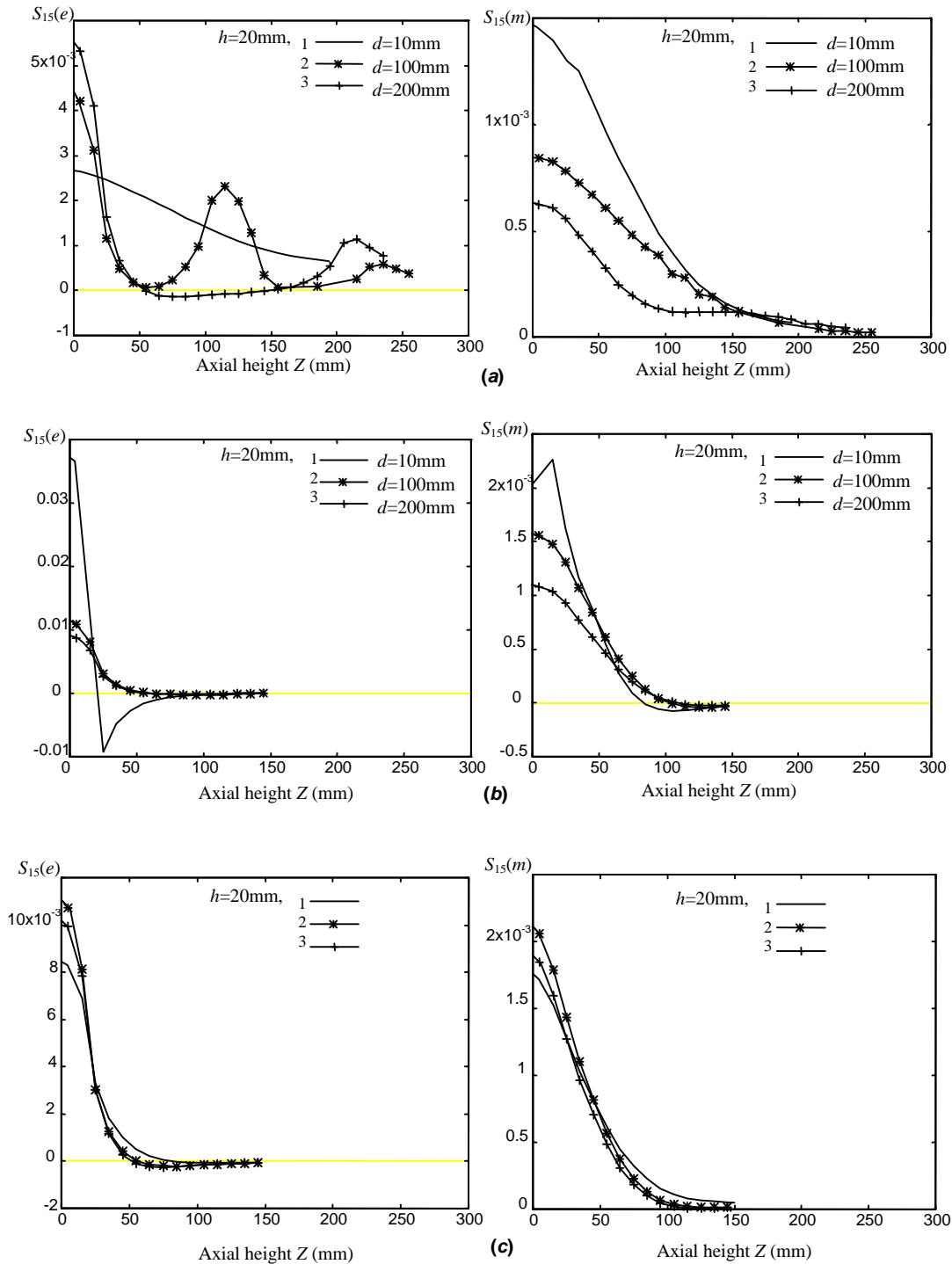


**Figure 2: Sensitivities at positions near the active electrode and near the Z-axis along axial direction**  
**(a) Sensor structure type 1; (b) Type 2; (c) Type 3**

## 6. IMAGE RECONSTRUCTION

To compare the properties of these sensor structures, a roping flow regime is used as physical phantom. The flow is moving around the Z-axis, and the distance between the centre of the rope and the centre of the flow (i.e. the Z-axis) is  $R_1/2$ . In the measurement electrode level, the centre of the rope is located at  $(\bar{x}, y) = (R_1/2, R_1/2)$ . The cross-sectional area of the rope is about 4.7% of  $R_1^2$ . The improved LBP reconstruction algorithm is employed and three images at the measurement electrode level are plotted in Figure 5. The boundaries are not clear because of the inherent shortage of the algorithm. The SIEs are given without and with a threshold applied to the reconstructed images [5]. As there is no threshold being used, the SIE of sensor structure type 1 (see Figure 5(a)) is 6.88, and the SIEs of type 2 (Figure 5(b)) and type 3 (Figure 5(c)) are 5.21 and 4.99 respectively. While a threshold of  $\approx 0.8$  is employed to reduce the low grey-level artefacts presented in the images, the SIEs corresponding to these three sensor structures are 0.53, 0.82 and 0.52.

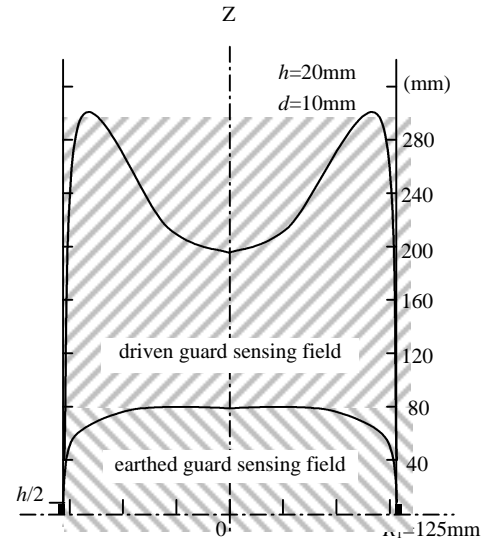


Figure 3: Sensing field of two sensor types

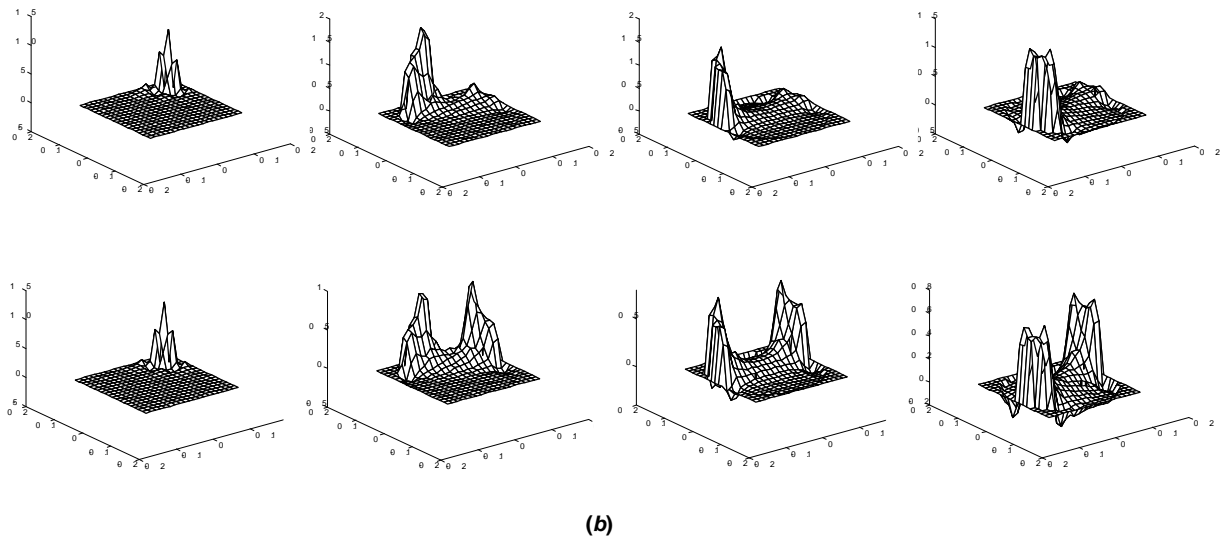


Figure 4: Sensitivity distributions of type 1 and type 2 on the measurement cross section

(a)  $S_{12}$ ,  $S_{13}$ ,  $S_{14}$  and  $S_{15}$  of type 1; (b)  $S_{12}$ ,  $S_{13}$ ,  $S_{14}$  and  $S_{15}$  of type 2

## 7. CONCLUSIONS

It can be concluded from the 3D FEM simulations that: (1) the widest range of sensitivity in axial direction is from the sensor structure with driven axial guards; (2) the smallest absolute change of capacitance ( $C(k) - C_0$ ) is from the sensor structure with earthed axial guard rings; (3) the largest ratio of the absolute

change ( $C(k) - C_0$ ) at the positions near the axis to the positions near the active electrode on the measurement cross-section (i.e. the XY plane) is from the sensor structure without any axial guard electrodes. And the results from the images reconstructed show that the sensor structure without any axial guard can present a similar image with the original phantom.

## REFERENCES

- [1] G. E. Fasching, W. J. Loudin and N. S. Smith, "Capacitive system for three-dimensional imaging of fluidized-bed density", *IEEE Trans. I&M*, 1994, **43**(1), pp.56-62
- [2] G. E. Fasching and N. S. Smith, "A capacitive system for three-dimensional imaging of fluidized beds", *Rev. Sci. Instrum.*, 1991, **62**(9), pp.2243-2251
- [3] F. T. Kuhn, J. C. Schouten, R. F. Mudde and C. M. van den Bleek, "Analysis of chaos in fluidization using electrical capacitance tomography", *Meas. Sci. Technol.*, 1996, **7**(4), pp.361-368
- [4] W. Q. Yang, W. F. Conway and M. S. Beck, "A demonstration unit for fluidisation process analysis with capacitance tomography", *Frontiers in Industrial Process Tomography-II*, pp.225-228, 9-12 April 1997, Delft, Netherlands
- [5] C. G. Xie, S. M. Huang, C. P. Lenn, A. L. Stott and M. S. Beck, "Experimental evaluation of capacitance tomographic flow imaging systems using physical models", *IEE Proc. G*, 1994, **141**(5), pp.357-368

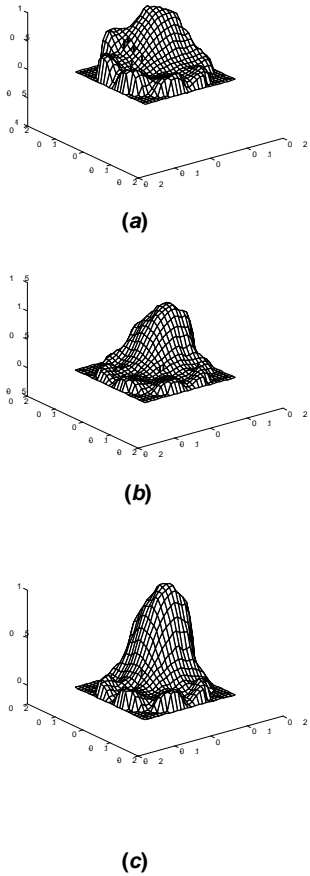


Figure 5: Images reconstructed with sensor structure type 1, type 2 and type 3

(a) With type 1; (b) With type 2; (c) With type 3